ACS SENSORS

Article

Cite This: ACS Sens. XXXX, XXX, XXX−XXX

pubs.acs.org/acssensors

Compact Grating-Coupled Biosensor for the Analysis of Thrombin

Daria Kotlarek,[†] Mariia Vorobii,[‡] Wojciech Ogieglo,[‡,§] Wolfgang Knoll,[†] Cesar Rodriguez-Emmenegger,[‡] and Jakub Dostálek*,[†]

[†]Biosensor Technologies, AIT-Austrian Institute of Technology GmbH, Konrad-Lorenz-Straße 24, 3430 Tulln an der Donau, Austria

[‡]DWI − Leibniz Institute for Interactive Materials and Institute of Technical and Macromolecular Chemistry, RWTH Aachen University, Forckenbeckstraße 50, 52074 Aachen, Germany

Supporting Information

ABSTRACT: A compact optical biosensor for direct detection of thrombin in human blood plasma (HBP) is reported. This biosensor platform is based on wavelength spectroscopy of diffraction-coupled surface plasmons on a chip with a periodically corrugated gold film that carries an antifouling thin polymer layer consisting of poly[(*N*-(2-hydroxypropyl)-methacrylamide)-*co*-(carboxybetaine methacrylamide)] (poly(HPMA-*co*-CBMAA)) brushes. This surface architecture provides superior resistance to nonspecific and irreversible adsorption of abundant compounds in the analyzed HBP samples in comparison to standard surface modifications. The carboxylate groups along the polymer brushes were exploited for the covalent immobilization of aptamer ligands. These ligands were selected to specifically capture the target thrombin analyte from the analyzed HBP sample in a way that does not activate the coagulatory process at the biosensor surface with poly(HPMA-*co*-CBMAA) brushes. Direct label-free analysis of thrombin in the medically relevant concentration range (1−20 nM) is demonstrated without the need for diluting the HBP samples or using additional steps for signal enhancement. The reported platform constitutes the first step toward a portable and sensitive point-of-care device for direct detection of thrombin in human blood.

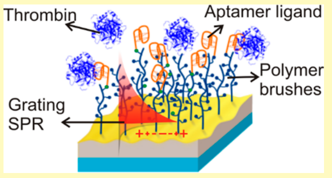

KEYWORDS: *surface plasmon resonance, grating-coupled surface plasmon resonance, biosensor, thrombin, antifouling brushes, aptamer, blood plasma, point of care*

Hemostasis is an indispensable physiological mechanism that maintains the integrity of the vascular system and circulation of the blood in the fluid state.[1] It relies on a number of highly regulated pro- and antithrombotic pathways that control the suppression of bleeding at the site of vessel injury, clot dissolution, and wound remodeling.[2] The delicate balance between coagulation and fibrinolytic activity can be disrupted by congenital and acquired coagulopathies,[1] anticoagulation therapy,[3] surgical procedures,[4,5] cardiopulmonary bypass,[6] and extracorporeal life support.[7] In these cases, the patient is exposed to a risk of life-threatening hemorrhage or a thrombotic event that requires immediate medical intervention. The incidence of hemostatic complications and their consequences (mortality, number of transfusions, time spent in the intensive care, cost of the treatment) can be substantially reduced by routine clinical diagnostics complemented by self-testing of a patient's coagulation status.[8−10] However, because of the complexity of the hemostatic system with a plentiful positive and negative feedback controls, a generic and widely accepted method for the assessment of coagulation stage does not exist neither at patient's home nor in clinical practice.[11]

Affinity optical biosensors based on surface plasmon resonance (SPR) are considered as among the prime candidates for "next-generation" diagnostic devices.[12] The SPR biosensors hold potential to serve in emerging point-of-care (POC) applications offering the advantage of fast response, real-time measurement, and already developed implementations to portable devices.[13] Up to now, portable systems based on the SPR biosensor principle were pursued for their applications in food safety,[14,15] environmental monitoring, biodefense,[16,17] and medical diagnostics.[18,19] The majority of the reported portable SPR devices rely on the Kretschmann configuration of the attenuated total reflection (ATR) enabling resonant excitation of propagating surface plasmons (PSPs) on the sensor surface with a continuous metallic film.[20,21] In order to simplify the use of SPR sensor chips in compact or portable reader devices, diffraction grating-coupled surface plasmon resonance (GC-SPR) provides an alternative to the ATR method.[22,23] The GC-SPR chips carry nanostructures that can be fabricated by scaled up means with injection molding,[24] roll-to-roll nanoimprint lithography,[25] or laser interference lithography.[26] These types of nanostructures were implemented to disposable sensor chips and used in the compact sensor designs supported by dedicated readers[27−29] as well as by optics integrated to smartphones.[30]

Throughout the last years, we witnessed a gradual progress in the development of thrombin biosensors based on electrochemical,[31] piezoelectric,[32] and optical transducers.[33] Among these, SPR biosensors reached the limit of detection at pico- and attomolar concentrations[34,35] and relied on readers

Received: May 6, 2019
Accepted: July 31, 2019
Published: July 31, 2019

with miniature design by using plasmonic nanostructures[36] or optical fibers.[37] Although detection of thrombin in the medically relevant range (5−20 nM) is well established in model samples, the operation in complex biological media such as human blood, plasma, and serum remains challenging due to the unspecific adsorption of matrix proteins to the sensor surface—a phenomenon also called "fouling". The fouling from blood plasma is the result of complex cooperative intermolecular interactions,[38] which constitutes a multiscale process that begins with adsorption of smaller proteins that are subsequently replaced by more surface-affine ones (Vroman effect[39]) and followed by the activation of different coagulatory factors as well as thrombocytes. In the SPR affinity biosensors, fouling severely complicates the discrimination between the response originating from the capture of the target analyte and the unspecific protein adsorption on the sensor surface and thus impairs their performance. The most common approach to reduce the protein fouling is a modification of the metallic surface with self-assembled monolayers (SAM) carrying oligo(ethylene glycol) moieties.[40] This modification typically provides good resistance to the fouling from model samples; however, it is not sufficient when the sensor surface is challenged with more complex bodily fluids.[41] The often used strategy to mitigate the effect of unspecific interactions is diluting the analyzed sample tens to hundreds of times with a reaction buffer,[42,43] which lowers the concentration of the target analyte that is available for the detection by the same factor. In addition, multiple-step assays with the enhancement of specific response by using the sandwich assay format combined with metallic nanoparticles were reported,[43] and advanced reference-compensated measurement strategies were pursued.[44] Despite these advances in SPR biosensor technology, only one of the aforementioned studies achieved a sufficient limit of detection (LOD) of thrombin in 10% serum for the prediction of the thrombotic event by the combined aptamer-based rolling circle amplification and bio-bar-coded AuNP enhancement.[35]

Notably, the SPR analysis of complex biological media can be simplified by the implementation of an antifouling biointerface architecture that will resist the biological matrix effect and thus enable the specific detection of the target analyte without the need of sample dilution or signal amplification. The poly[(*N*-(2-hydroxypropyl)-methacrylamide)-*co*-(carboxybetaine methacrylamide)] (poly-(HPMA-*co*-CBMAA)) brushes have become among the most successful strategies for eliminating protein adsorption on the sensor surface from blood serum and plasma[45−47] and saliva.[48] Most importantly, the immobilization of the receptor molecules to these poly(HPMA-*co*-CBMAA) brushes induces only minute changes in their structure, and thus, it minimally impairs their antifouling properties. This functionality was demonstrated for brushes prepared by statistical copolymerization of two antifouling monomers HPMA and CBMAA (85:15%) that provides a small fraction of side groups available for functionalization with receptors.[45]

In this study, we address the important clinical need for a compact device to monitor the concentration of thrombin in biological media by developing a compact plasmonic biosensor. It should be emphasized that the detection of thrombin in the blood plasma is particularly challenging because its capture on the sensor surface locally increases its concentration and can trigger the coagulation cascade. Therefore, the surface of a diffraction grating was coated with an advanced biointerface architecture comprising poly-(HPMA-*co*-CBMAA) brushes that were post modified with an aptamer ligand. The single-stranded DNA aptamer used in this study binds to exosite I of thrombin by adopting a G-quadruplex conformation leading to inhibition of thrombin-catalyzed clot formation.[49,50] In addition, we used a univalent thrombin inhibitor—argatroban—in order to prevent the coagulation of the bulk human blood plasma (HBP) sample. Argatroban binds to the active site of thrombin blocking the catalytic activity of soluble and fibrin-bound thrombin and reducing thrombin-mediated activation of platelets.[51] By occupying the active site only, argatroban does not impair the recognition of thrombin by the surface-attached aptamer. The importance of antifouling sensor surface engineering is demonstrated by selective capture of medically relevant concentrations of thrombin in undiluted HBP.

■ EXPERIMENTAL SECTION

Materials. Thrombin purified from human plasma (M_W = 37 kDa) was purchased from Enzo Life Sciences (Switzerland). The thrombin binding aptamer HD1 (amino modifier C6 5′-TTTTTGGTTGGTGTGGTTGG-3′) and control aptamer (scrambled sequence: amino modifier C6 5′-TTTTTGGTGGTGGTTGTGGT-3′) were synthesized by Integrated DNA Technologies (Belgium). The pooled normal HBP samples were obtained from Innovative Research (USA). Alkane PEG-thiol with a carboxylic acid group (carboxyl PEG-thiol, TH 003-m11.n6-0.1) was purchased from Prochimia (Poland), and (11-mercaptoundecyl)triethyleneglycol (hydroxyl PEG-thiol, SPT-0011) was purchased from SensoPath Technologies Inc. (USA). Buffer solutions were prepared by using ultrapure water (arium pro, Sartorius Stedim) with all reagents used as received unless otherwise stated. 2-(*N*-Morpholino)ethanesulfonic acid (MES), acetic acid, sodium acetate (SA), sodium chloride, HEPES, PBS buffer tablets, and argatroban monohydrate (M_W = 526.65 g/mol) were purchased from Sigma-Aldrich (Austria). 1-Ethyl-3-(3-dimethylaminopropyl)-carbodiimide (EDC) and *N*-hydroxysuccinimide (NHS) were obtained from Thermo Scientific (Austria). $CuCl_2$ (99.999%) and 1,4,8,11-tetramethyl-1,4,8,11-tetraazacyclotetradecane (Me_4Cyclam, 98%) were purchased from Sigma-Aldrich (Germany). CuCl was purchased from abcr GmbH (Germany). Methanol (MeOH) and ethanol (EtOH) were purchased from VWR Chemicals (Germany). Milli-Q water for the polymer synthesis was obtained using an Elga US filter Purelab Plus UF purification system (PL5113 02) (U.K.).

Preparation of Plasmonic Gratings. A master structure of crossed relief grating was prepared by UV laser interference lithography as described before.[52] It was cast to poly-(dimethylsiloxane) (PDMS, Sylgard 184 from Dow Corning, USA), which was cured overnight at 60 °C. The PDMS structure was detached from the master and used as a working stamp for further replication by UV-nanoimprint lithography. The UV-curable polymer Amonil MS10 (Amo GmbH, Germany) was spun on a BK7 glass substrate at 3000 rpm for 120 s. The PDMS working stamp was placed on the top of the Amonil layer, and the polymer was irradiated with UV light at λ = 365 nm with an irradiation dose of 2 J/cm^2 (UV lamp Bio-Link 365, Vilber Lourmat). Then the PDMS stamp was released from the UV-cured Amonil layer leaving an imprinted pattern of the master structure on the BK7 glass substrate. Subsequently, chromium (4 nm thickness) and gold (100 nm thickness) layers were deposited on the Amonil grating by vacuum thermal evaporation (HHV AUTO 306 from HHV LTD, U.K.) in vacuum better than 10^{-6} mbar. The prepared GC-SPR sensor chips comprised an area that was structured and area that was flat and served as a reference in the optical measurements.

Synthesis of Poly(HPMA-*co*-CBMAA) Brushes. ω-Mercaptoundecyl bromoisobutyrate and *N*-(2-hydroxypropyl)methacrylamide (HPMA) were synthesized according to the literature.[53,54] (3-Methacryloylaminopropyl)-(2-carboxyethyl)-dimethylammonium

DOI: 10.1021/acssensors.9b00827
ACS Sens. XXXX, XXX, XXX−XXX

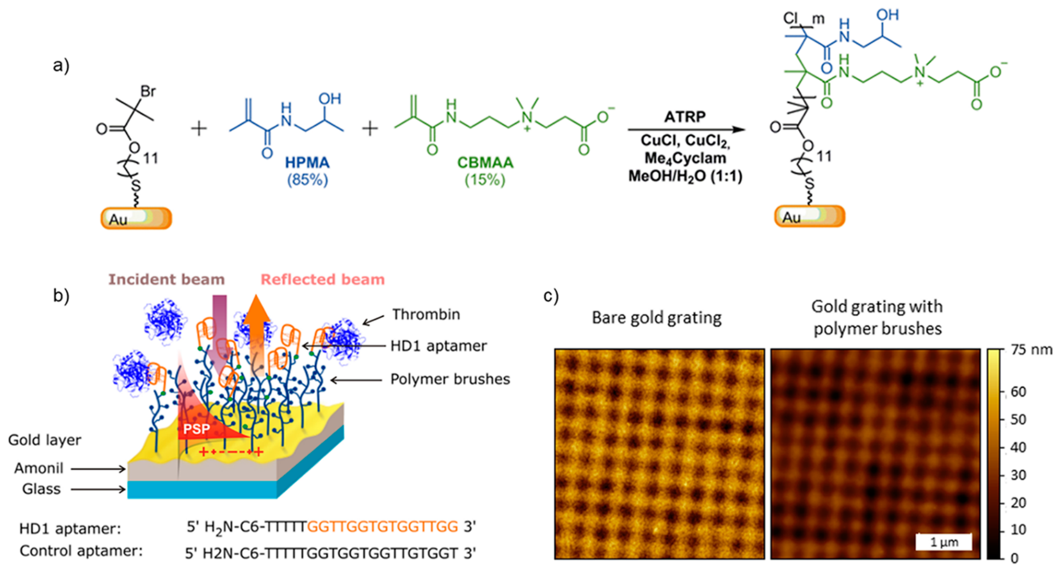

Figure 1. (a) Synthesis and chemical structure of poly(HPMA-*co*-CBMAA) brushes on a gold surface by ATRP. (b) Sensor chip surface with corrugated gold layer carrying nonfouling poly(HPMA-*co*-CBMAA) brushes for detection of thrombin. (c) AFM observation of the bare gold grating and the grating coated with polymer brushes.

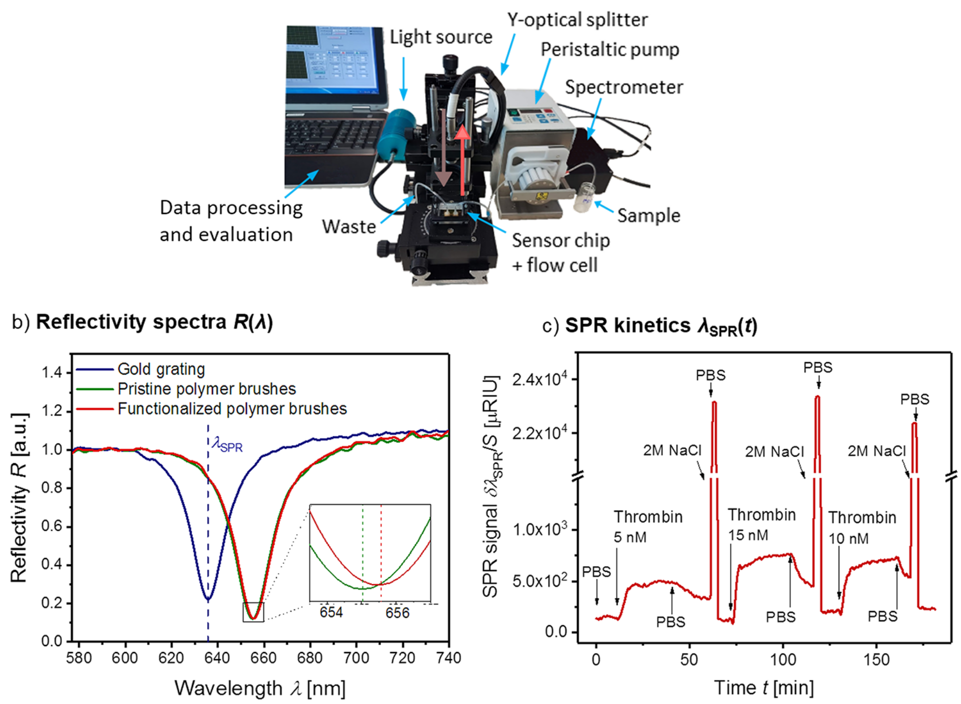

Figure 2. (a) Photograph of the compact GC-SPR instrument. (b) SPR spectra obtained from the gold grating, grating modified with pristine polymer brushes, and after the immobilization of the aptamer. (c) Sensorgram showing detection of thrombin in PBS by using a plasmonic grating chip modified with poly(HPMA-*co*-CBMAA) brush and HD1 aptamer.

(carboxybetaine methacrylamide, CBMAA) was synthesized using a modification of a procedure reported earlier.[55] Shortly, the GC-SPR sensor chips with the gold film were immersed in 2.4 mM solution of ω-mercaptoundecyl bromoisobutyrate in EtOH overnight to form SAM of the initiator. For the atom transfer radical polymerization (ATRP), 8 mL of MeOH and 8 mL of Milli-Q water were degassed in separated Schlenk flasks via seven freeze−pump−thaw cycles. Simultaneously, catalyst [$CuCl_2$ (6.1 mg, 78 μmol), CuCl (20.5 mg, 207 μmol), and Me_4Cyclam (70.6 mg, 275 μmol)] and monomers [HPMA (1.4 g, 9.7 mmol) and CBMAA (409 mg, 1.7 mmol)] were placed in separated Schlenk flasks and degassed by a pump and refilled. Subsequently, 4 mL of MeOH and 7 mL of Milli-Q water together with 3 mL of MeOH were transferred to the Schlenk flasks containing the catalyst and monomers under a N_2 atmosphere and were stirred until all solids were dissolved. Then the obtained catalyst solution was mixed with the monomer solution using a gas-tight syringe under a N_2 atmosphere and transferred to previously degassed reactors containing the GC-SPR sensor chip with SAM. The polymerization was carried out at 30 °C for 2 h. The samples were taken out from the reactors, washed with EtOH and Milli-Q water, and dried with N_2. The scheme of the polymerization is shown in Figure 1a.

Morphology Measurements. The morphology of the crossed relief grating before and after the modification with poly(HPMA-*co*-

DOI: 10.1021/acssensors.9b00827
ACS Sens. XXXX, XXX, XXX−XXX

CBMAA) brushes was observed by using atomic force microscopy (AFM, PicoPlus from Molecular Imaging, Agilent Technologies, Germany) in the tapping mode with tips PPP-NCHR-50 (Nanosensors, Switzerland). The acquired images were analyzed with the open-source software Gwyddion (version 2.47 from gwyddion.net). The grafting of polymer brushes was monitored by measuring the thickness of the dried polymer film using a spectroscopic ellipsometer M2000 (J.A.Woollam Co., USA) operated in rotating compensator mode. All measurements were performed in air at room temperature in the wavelength range of 350−1000 nm with a Xe-arc lamp light source and angles of incidence of 65, 70, and 75°. The obtained data were analyzed with the CompleteEASE software using a transparent Cauchy-type optical dispersion to model the polymer brushes.

Optical Setup of GC-SPR Biosensor. The in situ probing of the sensor surface was performed by using an in-house developed compact instrument (Figure 2). The polychromatic light from a halogen light source (12 V, HL-2000, Mikropack, USA) was coupled to an input arm of a Y-optical fiber splitter (Ø 400 μm core, 0.39 NA, Thorlabs, U.K.). The light emitted from the output arm of the Y-optical splitter was collimated by using a lens (focal length of 11 mm, Thorlabs, U.K.) and made normally incident at the sensor surface in order to resonantly excite PSPs on its corrugated gold surface. A flow cell with a chamber depth of 100 μm, length of 10 mm, and width of 5 mm was clamped against the gold sensor surface in order to contain aqueous samples. The flow cell consisted of a thin PDMS gasket and a transparent glass with drilled input and output ports. The analyzed liquid samples were flowed through the flow chamber by using a peristaltic pump (Ismatec, Switzerland) with a flow rate of 50 μL/min. The light reflected from the sensor surface was coupled back to the Y-optical fiber splitter that was connected to a spectrometer (HR4000, OceanOptics Inc., USA). The measured spectrum of the light beam reflected from the grating surface was normalized with that acquired from the reference flat area on the sensor chip. The normalized reflectivity spectra $R(\lambda)$ were processed by a dedicated LabView software,[56] and the spectral position of the resonant coupling to PSPs λ_{SPR} was tracked as a function of time t (Figure 2). The acquisition time of the SPR reflectivity spectra was set at 7 ms, and 100 spectra were accumulated.

The changes in the spectral position of GC-SPR reflectivity dip $\delta\lambda_{SPR}$ were determined by fitting with an analytical function. The resonant wavelength shifts $\delta\lambda_{SPR}$ were calibrated by the measuring the sensor response to the flow of 1, 2, and 4 wt % water solutions of sucrose with known refractive indices ($\delta n_s = 1.4 \times 10^{-3}$, 2.8×10^{-3}, 5.6×10^{-3} RIU, respectively) in order to convert the sensor signal to refractive index units (RIU). The refractive index sensitivity was determined as $S = \delta\lambda_{SPR}/\delta n_s$. From the SPR signal baseline, the standard deviation $\sigma[\lambda_{SPR}(t)]$ of its noise was obtained, and the refractive index resolution was obtained as σ/S.

Immobilization of Aptamers. The HD1 or control aptamers with the amine terminal group were covalently coupled to the carboxylic groups carried by the poly(HPMA-*co*-CBMAA) brushes. The coupling was monitored in situ by the use of GC-SPR, and first, the baseline in $\lambda_{SPR}(t)$ was established upon a flow of PBS (pH 7.4). Then the surface was incubated with 10 mM SA buffer (pH 5.0) for 5 min, and a freshly prepared solution of EDC (0.4 M) and NHS (0.1 M) in 50 mM MES buffer (pH 6.0) was reacted with the brushes for 10 min in order to activate the carboxylic groups. Subsequently, the surface was rinsed with 10 mM SA (pH 5.0) and HEPES (pH 7.5) for 1 min each. The activated surface was exposed to 1 μM solution of the aptamer for 30 min and rinsed with HEPES (pH 7.5) for 5 min. Finally, the functionalized sensor surface was washed with PBS (pH 7.4) for 90 min to let the unreacted active ester groups hydrolyze.

Observation of the Fouling. The fouling from undiluted HBP was monitored by using a GC-SPR instrument. Four types of GC-SPR sensor chips with different surface chemistries were examined: unmodified gold, gold surface with a mixed SAM (formed upon overnight incubation in ethanolic solution with dissolved carboxyl PEG-thiol and hydroxyl PEG-thiol at ratio 1:10, respectively, and 1 mM total concentration), gold surface with pristine poly(HPMA-*co*-CBMAA) brushes, and gold surface with poly(HPMA-*co*-CBMAA) brushes that were functionalized with the HD1 aptamer. For each surface chemistry, a baseline in SPR signal $\lambda_{SPR}(t)$ in PBS (pH 7.4) was established for 5 min. Then undiluted HBP that was spiked with 1 μL of argatroban monohydrate (stock 10 mg/mL) in a final volume of 500 μL was flowed over each surface for 15 min followed by the rinsing with PBS for 5 min. The amount of unspecifically bound species from HBP on the sensor surface was determined in ng/mm^2 from the difference in the sensor signal before λ_{SPR} and after the contact with the HBP as $\Gamma = 1.5{\cdot}\delta\lambda_{SPR}$ for polymer brushes and $0.85{\cdot}\delta\lambda_{SPR}$ for bare gold (SPR wavelength shift $\delta\lambda_{SPR}$ is in nm) based on numerical simulations discussed in the Supporting Information.

Detection of Thrombin. The sensor chips with poly(HPMA-*co*-CBMAA) brushes functionalized with an aptamer ligand (specific HD1 or scrambled HD1 sequence) were used to detect thrombin in analyzed liquid samples (Figure 1b). Two types of samples that were spiked with a known concentration of thrombin were prepared. The PBS sample was spiked with thrombin at concentrations of c = 1, 2.5, 5, 7.5, 10, 12.5, 15, 17.5, 20, 22.5, and 25 nM. 1 μL of argatroban stock solution (10 mg/mL, c = 19 mM) was added to the analyzed HBP sample, gently mixed, and incubated for 5 min. Afterward, the HBP sample was spiked with thrombin (stock 500 nM) to obtain c = 5, 10, 15, and 20 nM in a final sample volume of 500 μL and gently mixed prior to the analysis by using GC-SPR. The measurement baseline in the SPR sensor signal $\lambda_{SPR}(t)$ was established upon a 5 min flow of PBS. Then the sensor surface was exposed to the analyzed sample for 15 min and subsequently rinsed with PBS for 5 min. In order to regenerate the surface and release the affinity bound thrombin, aqueous solution with 2 M NaCl was flowed for 2 min. The sensor response ΔSPR was determined in μRIU from the difference in the SPR signal divided by refractive index sensitivity $\delta\lambda_{SPR}(t)/S$ before and after the target analyte binding. Similarly, two types of control experiments were performed. All measurements carried out in HBP were repeated three times in order to determine the standard deviation of the sensor response ΔSPR. The measured dependence of sensor response ΔSPR on the thrombin concentration c was fitted with Langmuir isotherm analytical function $\Delta SPR = \Delta SPR_{max}{\cdot}c/K_d/(1 + c/K_d)$, where ΔSPR_{max} is the response in saturation and K_d is the equilibrium dissociation affinity constant. The limit of detection (LOD) was defined as a concentration where 3 times the standard deviation of the baseline signal $3 \times \sigma[\lambda_{SPR}(t)]$ intersects the Langmuir fit of the calibration curve.

RESULTS AND DISCUSSION

Characterization of the Compact Sensor and Its Chips. The crossed relief grating structure was fabricated by using the UV-nanoimprint lithography followed by the coating with a 100 nm thick gold layer in order to resonantly couple the incident light beam to PSPs. The polymer brushes were subsequently synthesized on top of the gold film in order to provide a biointerface resistant to fouling from HBP. The surface of the diffraction grating with and without polymer brushes was analyzed by AFM as shown in Figure 1c. The period of the gold-coated grating with the sinusoidal profile was determined as $\Lambda = 434 \pm 16$ nm, and the corrugation depth was $h = 29.5 \pm 3.5$ nm. After the synthesis of the polymer brushes with a thickness of $d = 35 \pm 7$ nm, the grating corrugation depth decreased to $h = 13.2 \pm 1.6$ nm and reduced roughness of the topography was observed (Figure S1). These phenomena can be explained by the fact that, after their drying, the flexible polymer chains rearrange and tends to fill the concave areas of the grating.

The plasmonic grating structure on the top of the sensor chip was attached to a flow cell and loaded to the compact optical reader (see Figure 2a). The resonant excitation of PSPs on the bare gold grating is manifested as a narrow dip in the wavelength reflectivity spectrum $R(\lambda)$. It occurs at a wavelength λ_{SPR} where the normally incident wave and PSPs are

DOI: 10.1021/acssensors.9b00827
ACS Sens. XXXX, XXX, XXX−XXX

phase-matched due to the diffraction on the grating periodic corrugation. The momentum of the PSP waves is equal to the grating momentum $\mathrm{Re}\{k_{PSP}(\lambda)\} = 2\pi/\Lambda$ for the herein used first diffraction order coupling, which is fulfilled at a wavelength λ_{SPR} = 635.8 nm (see the spectral position of the reflectivity dip in Figure 2b). After the synthesis of poly-(HPMA-*co*-CBMAA) brushes on the top of the gold grating, the resonant wavelength shifts to λ_{SPR} = 655.1 nm due to an increase of the surface mass density Γ.

Importantly, the presence of polymer brushes (with a thickness of d = 35 nm) affects the sensitivity of the SPR sensor S to the refractive index changes occurring on its surface. The reason is that the polymer occupies part of the volume that is probed by the evanescent field of PSPs with a decay length L_p of ~100 nm. By measuring the detuning of λ_{SPR} due to the refractive index change n_s of an aqueous solution spiked with sucrose (Figure S2), the sensitivity of S = 459 ± 20 nm/RIU was determined for the GC-SPR chip without the polymer brushes. This value agrees with previous GC-SPR measurements at a similar wavelength.[56] On the same chips that carried the polymer brush biointerface architecture, the sensitivity decreased about twice to S = 238.3 ± 5.4 nm/RIU. The baseline of the SPR sensor signal exhibited the noise with a standard deviation σ of 3×10^{-3} nm, which translates to instrument refractive index resolutions of 6×10^{-6} RIU without the brushes and 1.1×10^{-5} ± RIU with the brushes. It is worth noting that more than an order of magnitude better resolution can be achieved with more advanced engineering of the GC-SPR sensor instrument; however, more sophisticated stabilization (e.g., temperature) has to be implemented.[29]

Immobilization of the Aptamers. In order to allow for the specific capture of the target analyte at the sensor surface, the aptamer receptors were tethered to polymer brushes. The immobilization of the thrombin-specific HD1 aptamer or scrambled control aptamer was performed in situ and monitored by GC-SPR. The reflectivity spectra $R(\lambda)$ (Figure 2b) and respective SPR sensor signal kinetics $\lambda_{SPR}(t)$ (Figure S3a) show that, after the immobilization of the aptamer, the resonance shifts to longer wavelengths. After 30 min, noncovalently bound aptamers were washed from the surface with a PBS buffer. A shift in the position of the SPR resonance $\Delta\lambda_{SPR}$ of about 0.5 nm was observed after the immobilization of the HD1 aptamer on the sensor surface, which corresponds to 2.3 ± 0.9 mRIU for the HD1 thrombin specific aptamer and 2.4 ± 0.1 mRIU for the scrambled sequence of the HD1 aptamer (Figure S3b).

Investigation of the Fouling of Biointerface Architectures. The fouling from undiluted HBP was observed from the SPR signal measured upon the contact of the sensor surface with a sample, and it was quantified in terms of the surface mass density change Γ determined after the rinsing of the surface with PBS. Besides the polymer-brush-coated gold grating surfaces, also sensor chips carrying a layer of bare gold and gold modified with PEG-thiol SAM were examined for comparison. Figure 3a shows the SPR sensor signal measured upon the 15 min flow of HBP over each type of surface followed by the rinsing. These data reveal that the injection of HBP rapidly shifts the SPR wavelength due to the bulk refractive index change Δn_s. Afterward, there is a slower gradual increase in the SPR signal on the bare and PEG-thiol modified gold surface due to the adsorption of HBP constituents. Importantly, much smaller gradual changes in the SPR signal are measured on the polymer brushes, which

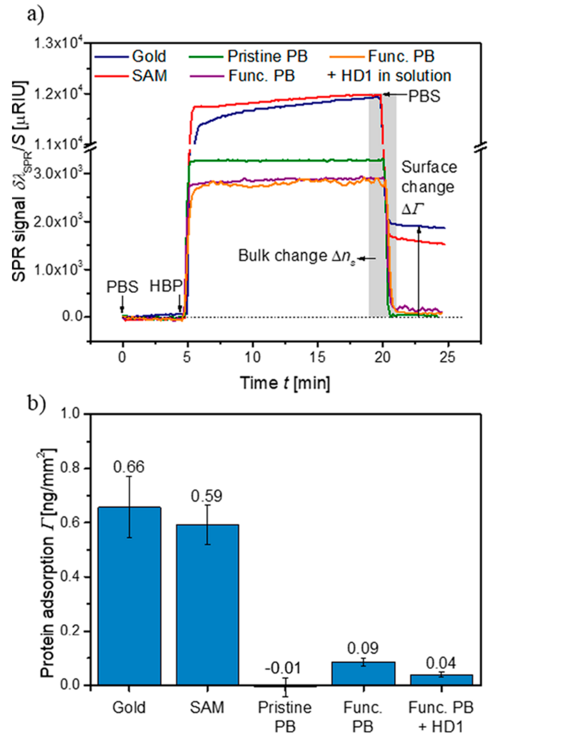

Figure 3. (a) Sensorgram showing fouling of the examined surfaces from 100% plasma with 38 μM argatroban: gold - bare gold, SAM - gold modified with a thiol-based SAM, pristine PB - gold modified with polymer brushes, func. PB - gold modified with polymer brushes that were functionalized with HD1 aptamer. (b) Averaged protein adsorption Γ reflecting fouling of each surface from 100% plasma with 38 μM argatroban.

indicate weaker unspecific interaction with HBP. After the rinsing with PBS, the SPR signal rapidly decreases owing to a change in the bulk refractive index Δn_s, and it reaches an equilibrium after 5 min. The surface mass density of the irreversibly deposited constituents Γ was determined from the change in the SPR signal baseline before and after the exposure to HBP as summarized in Figure 3b. In agreement with the previous studies,[46] there was no measurable change in Γ for pristine brushes demonstrating that the antifouling properties are not affected by the grating topology (Γ < 0.02 ng/mm²). These characteristics are superior to those measured for bare gold (Γ = 0.66 ng/mm²) and conventional gold modified with PEG-thiol SAM (Γ = 0.59 ng/mm²).

However, in contrast to a previous study[45] (in which a protein ligand was immobilized to similar brushes), we observed a significant increase in the surface mass density (Γ = 0.09 ng/mm²) for the brushes that were functionalized with the HD1 DNA aptamer. This observation indicates that the presence of negatively charged DNA strands can impair more severely the antifouling properties, but it also can be attributed to the capture of endogenous thrombin that is natively present in the tested pooled HBP at pM concentrations.[57,58] In order to elucidate between these two possible contributions, we measured the fouling for the HD1 aptamer-functionalized brushes from HBP that was spiked with the same HD1 aptamer. Then we observed about 2 times lower surface mass density increase (Γ = 0.04 ng/mm²), which can be ascribed to the blocking of the thrombin present in the sample and thus preventing its specific capture by the sensor HD1 aptamer tethered to the surface. Therefore, about 50% of the observed

DOI: 10.1021/acssensors.9b00827
ACS Sens. XXXX, XXX, XXX−XXX

SPR response can be ascribed to the fouling, and it should be highlighted that it corresponds to about 7% of the value observed on (even nonfunctionalized) PEG-thiol SAM that is widely accepted as the standard low-fouling surface architecture.

Detection of Thrombin. The developed GC-SPR sensor chip with poly(HPMA-*co*-CBMAA) brushes was used for the detection of thrombin in model PBS and undiluted HBP samples. The polymer brushes were functionalized either with thrombin-specific aptamer HD1 or by an aptamer with a scrambled sequence of nucleotides serving as a negative control. A series of HBP samples spiked with 38 μM argatroban and thrombin in the concentration range from c = 1 to 25 nM were prepared. The impact of argatroban on a thrombin detection assay was investigated, and it was confirmed that argatroban does not interfere with the aptamer binding site (Figure S4). As can be seen in Figures 2c and 4a, prepared samples were subsequently analyzed with the SPR sensor signal λ_{SPR}/S acquired in time. Each sample was flowed through the sensor for 15 min followed by rinsing with PBS and regeneration of the surface by introducing an aqueous solution of NaCl (2 M), which weakens the thrombin−HD1 affinity binding. Importantly, the regeneration of the surface with polymer brushes has been complete and leads to washing off of all the specifically captured thrombin as well as unspecifically adsorbed abundant HBP constituents. The control experiment was performed analogously for sensor chips with the polymer brushes functionalized with a scrambled sequence of the HD1 aptamer that does not form a G-quadruplex structure, which is indispensable for the binding of thrombin.

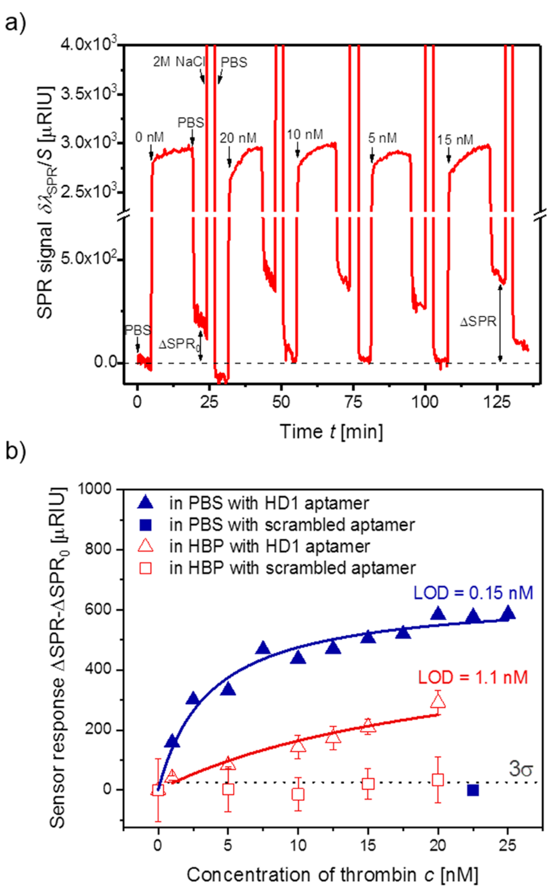

Figure 4. (a) Sensorgram showing detection of thrombin in 100% plasma. (b) Normalized SPR response vs concentration of thrombin measured in PBS (blue) (n = 1) and 100% plasma (red) (n = 3) by using the brushes functionalized with HD1 aptamer (triangles) or with control aptamer (squares).

As indicated in Figure 4a, the sensor response ΔSPR due to the binding of thrombin was determined from the SPR signal changes before the injection of a sample and after the rinsing with PBS prior to the regeneration step. The calibration curves were established for detection of thrombin in PBS (blue symbols in Figure 4b) and HBP (red symbols in Figure 4b). These data were fitted by using the Langmuir isotherm, and the obtained dissociation equilibrium constants were K_d = 3.7 and 22 nM for the PBS and HBP samples, respectively. Such variation can be attributed to potential interaction of the immobilized HD1 aptamer with other constituents that are present in HBP and not in PBS. These can include the background thrombin level in used pooled plasma (which would lead to false concentration of thrombin) and to the presence of ions and macromolecules that amend the balance of aptamer intermolecular interactions. It is worth noting that the obtained K_d values fall in the range that was reported in the literature and measured by using similar aptamers that were utilized for heterogeneous assays[59,60] as well as for homogeneous assays.[61,62] By taking into account the noise of the sensor signal, the limit of detection was determined as LOD = 0.15 and 1.1 nM for the PBS and HBP, respectively. In addition, squares in Figure 4b represent two control experiments obtained with the scrambled aptamer sequence in PBS (blue color) and human plasma (red color). An additional control experiment was performed by using HBP samples containing 38 μM argatroban that were spiked with 1 μM HD1 or scrambled control aptamer (Figure S5). The obtained data are in good agreement with the values that were obtained in the direct assay in HBP and confirm the specificity of the developed biosensor.

■ CONCLUSIONS

An optical biosensor platform for rapid direct monitoring of thrombin in human blood plasma was established based on grating-coupled SPR readout. The specific detection of thrombin that is not impeded by the interfering adsorption of proteins from human blood plasma was achieved by using the thrombin aptamers and advanced biointerface architecture comprising nonfouling poly(HPMA-*co*-CBMAA) brushes. We demonstrated that the label-free detection of thrombin content in undiluted human blood plasma is possible in 15 min with an LOD of 1.1 nM. The grating-coupled SPR sensor was implemented to a compact portable system making its deployment outside specialized optical laboratories possible. The further miniaturization of each individual component of the optical system can be pursued by future optoelectrical engineering paving the way toward handheld POC devices. Despite that further investigations are needed to be carried out (including tests on clinical samples) in order to evaluate the diagnostic value of the presented biosensor, the reported performance shows that the implementation of this technology to a diagnostic tool to monitor the coagulation status of patients at risk of thrombosis is possible. The coagulation process occurs once the level of thrombin in blood has reached approximately 5−20 nM,[63,64] and at the end of the clot formation, the concentration of thrombin can reach several hundred nM.[65] Therefore, the level of thrombin in the range of

DOI: 10.1021/acssensors.9b00827
ACS Sens. XXXX, XXX, XXX−XXX

5−20 nM indicates a high risk of thrombosis, and these values are within the detection range of the reported sensor.

■ ASSOCIATED CONTENT

Supporting Information

The Supporting Information is available free of charge on the ACS Publications website at DOI: 10.1021/acssensors.9b00827.

Topography changes of grating corrugation after the coating with antifouling polymer brushes and calibration of the sensor. GC-SPR sensorgrams for the functionalization of sensor chips together with the impact of argatroban on the assay performance and control thrombin assay. Numerical simulations of SPR sensor response in order to determine changes in the surface mass density from variations in the resonant GC-SPR wavelength (PDF)

■ AUTHOR INFORMATION

Corresponding Author

*E-mail: jakub.dostalek@ait.ac.at. Phone: +43 (0) 50550 4470. Fax: +43 (0) 50550 4450.

ORCID

Wojciech Ogieglo: 0000-0002-5335-9725

Cesar Rodriguez-Emmenegger: 0000-0003-0745-0840

Jakub Dostálek: 0000-0002-0431-2170

Present Address

[§]Advanced Membranes & Porous Materials Center, 4700 King Abdullah University of Science and Technology (KAUST), Thuwal 23955-6900, Kingdom of Saudi Arabia (W.O.).

Notes

The authors declare no competing financial interest.

■ ACKNOWLEDGMENTS

This project has received funding from the European Union's Horizon 2020 Research and Innovation Programme under grant agreement number 642787, Marie Sklodowska-Curie Innovative Training Network BIOGEL. C.R.-E. and M.V. acknowledge the support of the Deutsche Forschungsgemeinschaft (DFG) in the framework of the priority programme 2014 "Towards an Implantable Lung", with project numbers 346972946 and 347367912.

■ REFERENCES

(1) Rasche, H. Haemostasis and Thrombosis: An Overview. *Eur. Heart J. Suppl.* **2002**, *3*, 3−7.

(2) Sira, J.; Eyre, L. Physiology of Haemostasis. *Anaesth., Intensive Care Med.* **2016**, *17*, 79−82.

(3) Miyares, M. A.; Davis, K. Newer Oral Anticoagulants: A Review of Laboratory Monitoring Options and Reversal Agents in the Hemorrhagic Patient. *Am. J. Health-Syst. Pharm.* **2012**, *69*, 1473−1484.

(4) Adams, G. L.; Manson, R. J.; Turner, I.; Sindram, D.; Lawson, J. H. The Balance of Thrombosis and Hemorrhage in Surgery. *Hematol. Oncol. Clin. North Am.* **2007**, *21*, 13−24.

(5) Falck-Ytter, Y.; Francis, C. W.; Johanson, N. A.; Curley, C.; Dahl, O. E.; Schulman, S.; Ortel, T. L.; Pauker, S. G.; Colwell, C. W. Prevention of VTE in Orthopedic Surgery Patients: Antithrombotic Therapy and Prevention of Thrombosis. *Chest* **2012**, *141*, e278S−e325S.

(6) Edmunds, L. H., Jr; Colman, R. W. Thrombin During Cardiopulmonary Bypass. *Ann. Thorac. Surg.* **2006**, *82*, 2315−2322.

(7) Mazzeffi, M.; Greenwood, J.; Tanaka, K.; Menaker, J.; Rector, R.; Herr, D.; Kon, Z.; Lee, J.; Grif, B.; Rajagopal, K.; et al. Bleeding, Transfusion, and Mortality on Extracorporeal Life Support: ECLS Working Group on Thrombosis and Hemostasis. *Ann. Thorac. Surg.* **2016**, *101*, 682−689.

(8) Cortelazzo, S.; Finazzi, G.; Viero, P.; Galli, M.; Remuzzi, A.; Parenzan, L.; Barbui, T. Thrombotic and Hemorrhagic Complications in Patients with Mechanical Heart Valve Prosthesis Attending an Anticoagulation Clinic. *Thromb. Haemostasis* **2018**, *70*, 316−320.

(9) Despotis, G. J.; Joist, J. H.; Goodnough, L. T. Monitoring of Hemostasis in Cardiac Surgical Patients: Impact of Point-of-Care Testing on Blood Loss and Transfusion Outcomes. *Clin. Chem.* **1997**, *43*, 1684−1696.

(10) Heneghan, C.; Alonso-Coello, P.; Garcia-Alamino, J. M.; Perera, R.; Meats, E.; Glasziou, P. Self-Monitoring of Oral Anticoagulation: A Systematic Review and Meta-Analysis. *Lancet* **2006**, *367*, 404−411.

(11) Bashaw, M.; Triplett, S. Coagulopathy In and Outside the Intensive Care Unit. *Crit. Care Nurs. Clin. NA* **2017**, *29*, 353−362.

(12) Zheng, R.; Cameron, B. D. Surface Plasmon Resonance: Recent Progress toward the Development of Portable Real-Time Blood Diagnostics. *Expert Rev. Mol. Diagn.* **2014**, *12*, 5−7.

(13) Tokel, O.; Inci, F.; Demirci, U. Advances in Plasmonic Technologies for Point of Care Applications. *Chem. Rev.* **2014**, *114*, 5728−5752.

(14) Feltis, B. N.; Sexton, B. A.; Glenn, F. L.; Best, M. J.; Wilkins, M.; Davis, T. J. A Hand-Held Surface Plasmon Resonance Biosensor for the Detection of Ricin and Other Biological Agents. *Biosens. Bioelectron.* **2008**, *23*, 1131−1136.

(15) Wang, S.; Xie, J.; Jiang, M.; Chang, K.; Chen, R.; Ma, L.; Zhu, J.; Guo, Q.; Sun, H.; Hu, J. The Development of a Portable SPR Bioanalyzer for Sensitive Detection of Escherichia Coli O157:H7. *Sensors* **2016**, *16*, 1856.

(16) Mauriz, E.; Calle, A.; Montoya, A.; Lechuga, L. M. Determination of Environmental Organic Pollutants with a Portable Optical Immunosensor. *Talanta* **2006**, *69*, 359−364.

(17) Soelberg, S. D.; Furlong, C. E. Biosensors and Bioassays for Ecological Risk Monitoring and Assessment. In *Environmental Toxicology*; Springer: New York, 2013; pp 121−142.

(18) Prabowo, B. A.; Wang, R. Y. L.; Secario, M. K.; Ou, P. T.; Alom, A.; Liu, J. J.; Liu, K. C. Rapid Detection and Quantification of Enterovirus 71 by a Portable Surface Plasmon Resonance Biosensor. *Biosens. Bioelectron.* **2017**, *92*, 186−191.

(19) Trzaskowski, M.; Napiórkowska, A.; Augustynowicz-Kopeć, E.; Ciach, T. Detection of Tuberculosis in Patients with the Use of Portable SPR Device. *Sens. Actuators, B* **2018**, *260*, 786−792.

(20) Naimushin, A. N.; Soelberg, S. D.; Bartholomew, D. U.; Elkind, J. L.; Furlong, C. E. A Portable Surface Plasmon Resonance (SPR) Sensor System with Temperature Regulation. *Sens. Actuators, B* **2003**, *96*, 253−260.

(21) Stevens, R. C.; Soelberg, S. D.; Near, S.; Furlong, C. E. Detection of Cortisol in Saliva with a Flow-Filtered, Portable Surface Plasmon Resonance Biosensor System. *Anal. Chem.* **2008**, *80*, 6747−6751.

(22) Dostálek, J.; Homola, J.; Miler, M. Rich Information Format Surface Plasmon Resonance Biosensor Based on Array of Diffraction Gratings. *Sens. Actuators, B* **2005**, *107*, 154−161.

(23) Wang, Y.; Dostalek, J.; Knoll, W. Magnetic Nanoparticle-Enhanced Biosensor Based on Grating-Coupled Surface Plasmon Resonance. *Anal. Chem.* **2011**, 6202−6207.

(24) Arachchillage, D. R.; Passariello, M.; Laffan, M.; Aw, T. C.; Owen, L.; Banya, W.; Trimlett, R.; Morgan, C.; Patel, B. V.; Pepper, J.; et al. Intracranial Hemorrhage and Early Mortality in Patients Receiving Extracorporeal Membrane Oxygenation for Severe Respiratory Failure. *Semin. Thromb. Hemostasis* **2018**, *44*, 276−286.

(25) Kooy, N.; Mohamed, K.; Pin, L. T.; Guan, O. S. A Review of Roll-to-Roll Nanoimprint Lithography. *Nanoscale Res. Lett.* **2014**, *9*, 320.

DOI: 10.1021/acssensors.9b00827
ACS Sens. XXXX, XXX, XXX−XXX

(26) Lu, C.; Lipson, R. H. Interference Lithography: A Powerful Tool for Fabricating Periodic Structures. *Laser Photonics Rev.* **2010**, *4*, 568−580.
(27) Vala, M.; Chadt, K.; Piliarik, M.; Homola, J. High-Performance Compact SPR Sensor for Multi-Analyte Sensing. *Sens. Actuators, B* **2010**, *148*, 544−549.
(28) Fernández, F.; Hegnerová, K.; Piliarik, M.; Sanchez-Baeza, F.; Homola, J.; Marco, M. P. A Label-Free and Portable Multichannel Surface Plasmon Resonance Immunosensor for on Site Analysis of Antibiotics in Milk Samples. *Biosens. Bioelectron.* **2010**, *26*, 1231−1238.
(29) Piliarik, M.; Homola, J. Surface Plasmon Resonance (SPR) Sensors: Approaching Their Limits? *Opt. Express* **2009**, *17*, 16505.
(30) Zhang, J.; Khan, I.; Zhang, Q.; Liu, X.; Dostalek, J.; Liedberg, B.; Wang, Y. Lipopolysaccharides Detection on a Grating-Coupled Surface Plasmon Resonance Smartphone Biosensor. *Biosens. Bioelectron.* **2018**, *99*, 312−317.
(31) Centi, S.; Tombelli, S.; Minunni, M.; Mascini, M. Aptamer-Based Detection of Plasma Proteins by an Electrochemical Assay Coupled to Magnetic Beads. *Anal. Chem.* **2007**, *79*, 1466−1473.
(32) Bini, A.; Minunni, M.; Tombelli, S.; Centi, S.; Mascini, M. Analytical Performances of Aptamer-Based Sensing for Thrombin Detection. *Anal. Chem.* **2007**, *79*, 3016−3019.
(33) Pavlov, V.; Xiao, Y.; Shlyahovsky, B.; Willner, I. Aptamer-Functionalized Au Nanoparticles for the Amplified Optical Detection of Thrombin. *J. Am. Chem. Soc.* **2004**, *126*, 11768−11769.
(34) Baek, S. H.; Wark, A. W.; Lee, H. J. Dual Nanoparticle Amplified Surface Plasmon Resonance Detection of Thrombin at Subattomolar Concentrations. *Anal. Chem.* **2014**, *86*, 9824−9829.
(35) He, P.; Liu, L.; Qiao, W.; Zhang, S. Ultrasensitive Detection of Thrombin Using Surface Plasmon Resonance and Quartz Crystal Microbalance Sensors by Aptamer-Based Rolling Circle Amplification and Nanoparticle Signal Enhancement. *Chem. Commun.* **2014**, *50*, 1481−1484.
(36) Li, S.; Zhang, D.; Zhang, Q.; Lu, Y.; Li, N.; Chen, Q.; Liu, Q. Electrophoresis-Enhanced Localized Surface Plasmon Resonance Sensing Based on Nanocup Array for Thrombin Detection. *Sens. Actuators, B* **2016**, *232*, 219−225.
(37) Lao, J.; Han, L.; Wu, Z.; Zhang, X.; Huang, Y.; Tang, Y.; Guo, T. Gold Nanoparticle-Functionalized Surface Plasmon Resonance Optical Fiber Biosensor: In Situ Detection of Thrombin with 1 nM Detection Limit. *J. Lightwave Technol.* **2019**, *37*, 2748−2755.
(38) Andrade, J. D. *Surface and Interfacial Aspects of Biomedical Polymers: Volume 1 Surface Chemistry and Physics*; Springer Science & Business Media, 2012.
(39) Vroman, L.; Adams, A. L.; Fischer, G. C.; Munoz, P. C. Interaction of High Molecular Weight Kininogen, Factor XII, and Fibrinogen in Plasma at Interfaces. *Blood* **1980**, *55*, 156−159.
(40) Ostuni, E.; Chapman, R. G.; Holmlin, R. E.; Takayama, S.; Whitesides, G. M. A Survey of Structure-Property Relationships of Surfaces That Resist the Adsorption of Protein. *Langmuir* **2001**, *17*, 5605−5620.
(41) Rodriguez Emmenegger, C.; Brynda, E.; Riedel, T.; Sedlakova, Z.; Houska, M.; Alles, A. B. Interaction of Blood Plasma with Antifouling Surfaces. *Langmuir* **2009**, *25*, 6328−6333.
(42) Polonschii, C.; David, S.; Tombelli, S.; Mascini, M.; Gheorghiu, M. A Novel Low-Cost and Easy to Develop Functionalization Platform. Case Study: Aptamer-Based Detection of Thrombin by Surface Plasmon Resonance. *Talanta* **2010**, *80*, 2157−2164.
(43) Bai, Y.; Feng, F.; Zhao, L.; Wang, C.; Wang, H.; Tian, M.; Qin, J.; Duan, Y.; He, X. Aptamer/Thrombin/Aptamer-AuNPs Sandwich Enhanced Surface Plasmon Resonance Sensor for the Detection of Subnanomolar Thrombin. *Biosens. Bioelectron.* **2013**, *47*, 265−270.
(44) Špringer, T.; Bocková, M.; Homola, J. Label-Free Biosensing in Complex Media: A Referencing Approach. *Anal. Chem.* **2013**, *85*, 5637−5640.
(45) Riedel, T.; Surman, F.; Hageneder, S.; Pop-Georgievski, O.; Noehammer, C.; Hofner, M.; Brynda, E.; Rodriguez-Emmenegger, C.; Dostálek, J. Hepatitis B Plasmonic Biosensor for the Analysis of Clinical Serum Samples. *Biosens. Bioelectron.* **2016**, *85*, 272−279.
(46) Riedelová, Z.; Májek, P.; PeČánková, K.; KuČerová, J.; Surman, F.; De Los Santos Pereira, A.; Riedel, T. SPR Biosensor for Quantification of Fetuin-A as a Promising Multibiomarker. *Physiol. Res.* **2018**, *67*, 367−375.
(47) Vorobii, M.; Kostina, N. Y.; Rahimi, K.; Grama, S.; Söder, D.; Pop-Georgievski, O.; Šturcová, A.; Horak, D.; Grottke, O.; Singh, S.; et al. Antifouling Microparticles to Scavenge Lipopolysaccharide from Human Blood Plasma. *Biomacromolecules* **2019**, *20*, 959−968.
(48) Riedel, T.; Hageneder, S.; Surman, F.; Pop-Georgievski, O.; Noehammer, C.; Hofner, M.; Brynda, E.; Rodriguez-Emmenegger, C.; Dostálek, J. Plasmonic Hepatitis B Biosensor for the Analysis of Clinical Saliva. *Anal. Chem.* **2017**, *89*, 2972−2977.
(49) Bock, L. C.; Griffin, L. C.; Latham, J. A.; Vermaas, E. H.; Toole, J. J. Selection of Single-Stranded DNA Molecules That Bind and Inhibit Human Thrombin. *Nature* **1992**, *355*, 564−566.
(50) Paborskys, L. R.; Mccurdy, S. N.; Griffin, L. C.; Toole, J. J.; Leung, L. L. The Single-Stranded DNA Aptamer-Binding Site of Human Thrombin. *J. Biol. Chem.* **1993**, 20808−20811.
(51) Di Nisio, M.; Middeldorp, S.; Büller, H. R. Direct Thrombin Inhibitors. *N. Engl. J. Med.* **2005**, *353*, 1028−1040.
(52) Bauch, M.; Hageneder, S.; Dostalek, J. Plasmonic Amplification for Bioassays with Epi-Fluorescence Readout. *Opt. Express* **2014**, *22*, 32026.
(53) Jones, D. M.; Brown, A. A.; Huck, W. T. Surface-Initiated Polymerizations in Aqueous Media: Effect of Initiator Density. *Langmuir* **2002**, 1265−1269.
(54) Ulbrich, K.; Šubr, V.; Strohalm, J.; Plocová, D.; Jelínková, M.; Říhová, B. Polymeric Drugs Based on Conjugates of Synthetic and Natural Macromolecules. *J. Controlled Release* **2000**, *64*, 63−79.
(55) Rodriguez-Emmenegger, C.; Schmidt, B. V. K. J.; Sedlakova, Z.; Šubr, V.; Alles, A. B.; Brynda, E.; Barner-Kowollik, C. Low Temperature Aqueous Living/Controlled (RAFT) Polymerization of Carboxybetaine Methacrylamide up to High Molecular Weights. *Macromol. Rapid Commun.* **2011**, *32*, 958−965.
(56) Reiner, A. T.; Ferrer, N. G.; Venugopalan, P.; Lai, R. C.; Lim, S. K.; Dostálek, J. Magnetic Nanoparticle-Enhanced Surface Plasmon Resonance Biosensor for Extracellular Vesicle Analysis. *Analyst* **2017**, *142*, 3913−3921.
(57) Hemker, H. C.; Beguin, S. The Clotting Mechanism and How to Determine Its Phenotype. *Arch. Hell. Med.* **2000**, *17*, 13−18.
(58) Müller, J.; Becher, T.; Braunstein, J.; Berdel, P.; Gravius, S.; Rohrbach, F.; Oldenburg, J.; Mayer, G.; Pötzsch, B. Profiling of Active Thrombin in Human Blood by Supramolecular Complexes. *Angew. Chem., Int. Ed.* **2011**, *50*, 6075−6078.
(59) Müller, J.; Freitag, D.; Mayer, G.; Pötzsch, B. Anticoagulant Characteristics of HD1-22, a Bivalent Aptamer That Specifically Inhibits Thrombin and Prothrombinase. *J. Thromb. Haemost.* **2008**, *6*, 2105−2112.
(60) Pasternak, A.; Hernandez, F. J.; Rasmussen, L. M.; Vester, B.; Wengel, J. Improved Thrombin Binding Aptamer by Incorporation of a Single Unlocked Nucleic Acid Monomer. *Nucleic Acids Res.* **2011**, *39*, 1155−1164.
(61) Li, J. J.; Fang, X.; Tan, W. Molecular Aptamer Beacons for Real-Time Protein Recognition. *Biochem. Biophys. Res. Commun.* **2002**, *292*, 31−40.
(62) Zavyalova, E.; Tagiltsev, G.; Reshetnikov, R.; Arutyunyan, A.; Kopylov, A. Cation Coordination Alters the Conformation of a Thrombin-Binding G-Quadruplex DNA Aptamer That Affects Inhibition of Thrombin. *Nucleic Acid Ther.* **2016**, *26*, 299−308.
(63) Hemker, H. C.; Béguin, S. Thrombin Generation in Plasma: Its Assessment via the Endogenous Thrombin Potential. *Thromb. Haemostasis* **1995**, *74*, 134−138.
(64) Mann, K. G.; Brummel, K.; Butenas, S. What Is All That Thrombin For? *J. Thromb. Haemostasis* **2003**, *1*, 1504−1514.
(65) Brummel, K. E.; Paradis, S. G.; Butenas, S.; Mann, K. G. Thrombin Functions during Tissue Factor−Induced Blood Coagulation. *Blood* **2002**, *100*, 148−152.

DOI: 10.1021/acssensors.9b00827
ACS Sens. XXXX, XXX, XXX−XXX